

6 kHz MOPA light source for 193 nm immersion lithography

Walter D. Gillespie*, Toshihiko Ishihara, William N. Partlo, George X. Ferguson, Michael R. Simon
Cymer, Inc, 17075 Thornmint Ct., San Diego, CA 92127

ABSTRACT

Volume production immersion lithography scanners will require new light sources offering increased output power while delivering improved dose stability over a shorter exposure window. Scaling the light source repetition rate from 4 to 6 kHz is the logical step toward meeting those combined requirements. We will present the results of the latest progress towards developing a 193 nm, 6 kHz light source using Cymer's proprietary MOPA technology. We will discuss how the design of critical core technology elements, such as the discharge chamber, the solid-state-pulsed-power modules and opto-electronic detectors within the system are modified to handle the higher average power, thermal demands, and speed to support reliable operation up to 6kHz. The XLA platform, which is already used on three generations of 193 nm MOPA light source, allows seamless integration of these improved technology elements into a reliable, proven product platform. We will also report results of the characterization of the optical parameters critical to the lithography process, such as spectral bandwidth and its stability, energy stability and dose stability, up to 6 kHz.

Keywords: MOPA, ArF, excimer, high repetition rate

1. INTRODUCTION

With the development of immersion lithography scanners come requirements for new light sources offering increased output power and improved dose stability. To meet these demands, CYMER, Inc. is developing a new generation of 6 kHz, 193 nm excimer laser sources to be named the XLA-300.

The XLA-300 will build upon the technologies of its XLA model predecessors in that it will be based on the Master Oscillator-Power Amplifier (MOPA) architecture introduced in the XLA-100[1]. The XLA-300 will feature the Reduced Acoustic Peaks (RAP) chamber and the extended pulse stretcher introduced in the XLA-105, and it will also include the on-board E95 Bandwidth Analysis Module (BAM)[2], the increased available pulse energy and the lowered cost of operation from the XLA-200 system[3]. In addition to these features, however, the XLA-300 will introduce a re-designed line narrowing module (LNM) for a further reduction in spectral bandwidth to 0.12 pm and an increase in maximum repetition rate to 6 kHz. With available pulse energy of up to 15 mJ, this will result in a 90W ultra-line narrowed 193 nm immersion lithography tool. A summary of the planned specifications for the XLA-300 system is provided in Table 1.

Table 1. Summary of top level specifications for the XLA-300 laser.

Rep Rate, Energy and Power		
Power	W	90
Operational Energy Range (Total Range)	mJ	10.0 - 15.0
Rep Rate Range (OTS applies)	kHz	1.5 - 6.0
Pulse duration (TIS)	ns	> 72
Duty Cycle	%	75
Spectral Characteristics		
FWHM	pm	0.12
E95%	pm	0.25
E95% BW Stability	pm	0.05
ASE		<3 10 ⁻⁴
Energy/Dose Stability		
Dose stability	%	≤ +/- 0.10

* wgillespie@cymer.com; phone 858 385-7014; www.cymer.com

The increase in pulse repetition rate for the XLA-300 naturally impacts most major components of the laser. In particular, the discharge chamber, the pulsed power system, controls hardware and software, and the thermal management systems are all directly affected. In fact, certain aspects of the repetition rate increase indeed bring significant technical challenges, as discussed in previous work[4]. The fan power required to circulate the gas within the discharge chamber to maintain arc-free operation, for example, scales approximately as the cube of the repetition rate, such that a significant portion of the total laser input power threatens to be lost in circulation of the process gas. Also, the shorter inter-pulse interval leaves less time to dissipate acoustic disturbances generated by the discharge, leading to optical performance issues. Optical power loading on the line narrowing optics elements has been minimized through MOPA architecture, resulting in improved module lifetimes, reduced thermal transients and improved operational margin for output power. But electrical power loading in the pulsed power modules and discharge chamber at the higher repetition rate does present some design challenges. An evaluation of these challenges is presented below along with performance data from prototype 6 kHz systems, including energy and dose stability.

2. DISCHARGE CLEARING

Gain production in an excimer laser relies on an electrical discharge between two elongated electrodes in a halogen-rare gas mixture (the process gas). To sustain higher repetition rates, the discharge by-products (i.e. fluorine atoms, ions, electrode debris, etc.) must be swept away from the electrodes by a gas circulation system so that an essentially fresh gas mixture is available for every pulse. A cross-flow fan is used in Cymer chambers to circulate the process gas.

2.1. Arc-free operation

If fresh gas is not supplied, an even glow discharge cannot be maintained and filamentation of the glow discharge with corresponding reduced gain will result. Empirically, it has been found that the gas flow speed at the midpoint between the electrodes must be fast enough to advect the discharge by-products at least several discharge widths downstream to avoid "downstream arcing" (a phenomenon in which filaments from the discharge follow a curved path that stretches significantly downstream of the shortest distance between the anode cathode). The number of discharge widths for which no downstream arcing is observed is called the "clearing ratio" [5,6], and the minimum fan speed that achieves this clearing ratio is termed the Arc-Free Fan Speed (AFFS).

Not surprisingly, AFFS is a function of the laser repetition rate. Figure 1 shows measurements of AFFS for 3 operating voltages as a function of laser repetition rate. These measurements were made using an XLA-100 production standard chamber without flow improvements. As seen in the figure, the relationship between AFFS and repetition rate is roughly linear, but an apparent voltage dependence becomes stronger at higher repetition rates. Interestingly, the AFFS at 1150V, 6 kHz is not consistent with the trends seen at lower repetition rates. This may indicate a different phenomenology for arcing at 6kHz in this case, but experience with AFFS to 4 kHz has shown that a large number of factors influence AFFS behavior. Operating duty cycle, electrode wear, process gas pressure and fluorine content, pulsed power module variances, and chamber to chamber variability have all been seen to influence AFFS and its voltage dependence. Most significant from this data, then, is that the spread in AFFS increases with repetition rate. As a result, a larger margin above AFFS or tighter control of these variable factors will be required to ensure stable arc-free performance over the entire operating dynamic range. At 6 kHz, the increased margin required becomes a significant portion of the fan power budget, as will be seen below.

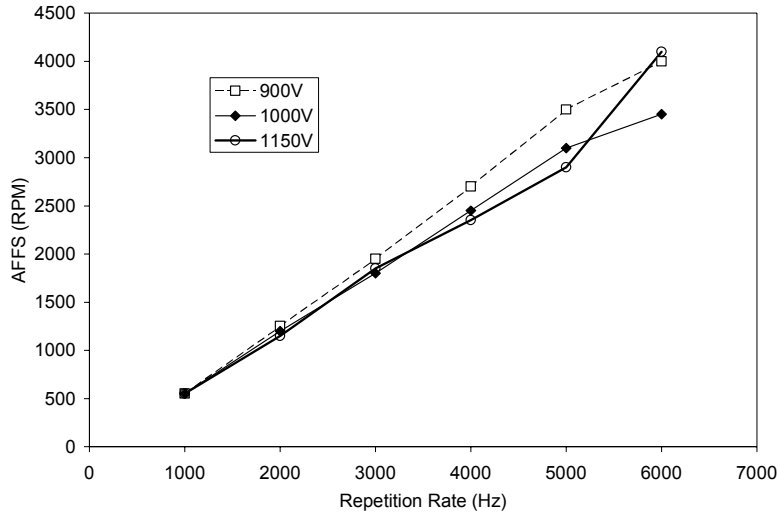


Figure 1. Arc-free fan speed as a function of laser repetition rate and laser operating voltage (V_{co}) for a single XLA-100 production chamber.

2.2. Fan Power

The fan power required to drive the flow at the AFFS shown in Figure 1 is charted in Figure 2. Because the power carried by a moving gas scales as the cube of the flow speed ($Power = \Omega \rho u^2 \sum \mu A$, where ρ = gas density, u = flow velocity and A = cross-sectional area through which the gas flows), and because the velocity required for arc-free performance is approximately linear with rep rate, we expect that the power required to drive the process gas in the chamber will scale approximately as the cube of the laser repetition rate. A cubic fit to the data is included in Figure 2 for reference.

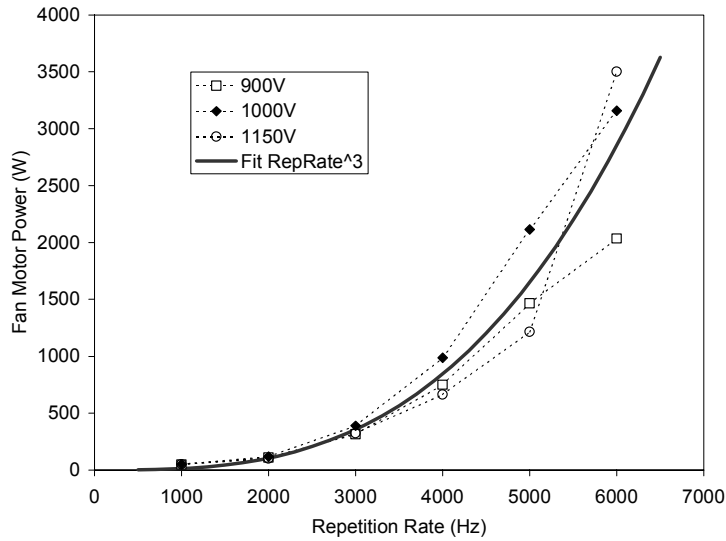


Figure 2. Fan motor power for the minimum fan speed to achieve arc-free performance.

Notable in the figure is that the fan power required to maintain arc-free performance at 6 kHz is more than a factor of 3 higher than the power required at 4 kHz. Also, the variance in AFFS at 6 kHz corresponds to nearly a factor of 2 in fan power. Considering that a reasonable margin against AFFS is required in normal laser operation to be certain that no arcing occurs, it is clear that the fan power requirements can quickly become quite large. One of Cymer's thrusts for

further development of next generation discharge chambers is toward reducing the variability in AFFS to allow lower fan speeds, which serves to reduce power, bearing wear, and chamber vibration.

Historically, fan power has not scaled as rapidly as the cube of repetition rate, however. A table of operating fan power for 5 generations of Cymer's ArF lasers is shown below. First, we note that the fan power requirement for a given repetition rate is considerably lower for ArF systems than for KrF systems (a corresponding table for KrF systems is presented in Ref[4]). This difference is primarily a consequence of the narrower discharge width in Cymer's ArF systems: recall that AFFS is dictated by discharge clearing, and a higher transverse flow speed is required to clear a wider discharge. Thus, from the standpoint of fan power, it is easier to achieve higher repetition rates in ArF systems than in KrF systems. Next, from the table, it can be noted that the fan power does not scale as the cube of the system's repetition rate; the increase in power requirements is much slower. The primary reason for this slower than predicted power increase is the development of improved flow geometries with each generation of discharge chamber. Work is currently underway at Cymer to further improve the flow efficiency for next generation 6 kHz chambers, but the XLA platform will already sustain the 5600 Watts of fan power required to operate at 6 kHz with current discharge chamber technology.

Table 2: Approximate fan power required for a series of Cymer's ArF excimer laser systems under normal operating conditions.

Model	Rep Rate	Fan Power
ELX-5000A	1000 Hz	400 W
ELS-6010A	2000 Hz	600 W
NL-7000/XLA-100	4000 Hz	2200 W
XLA-300	6000 Hz	5600 W

3. THERMAL MANAGEMENT

Only a small fraction of the electrical energy used by the laser is carried away as light output. In fact, typical electrical input to optical output efficiencies are on the order of a fraction of a percent for line-narrowed lasers. The remaining unused energy (up to 10 kW for 4kHz, 75% DC operation) is lost as heat that must be removed to maintain reliable laser operation. This section highlights some of the design improvements and engineering that will allow the XLA-300 to operate reliably at 6 kHz for lithography.

3.1. Solid State Pulsed Power

While the pulsed power modules have remained unchanged through the last three generations of XLA lasers, the increase to 6 kHz will require all new pulsed power modules. This includes the High Voltage Power Supply (HVPS), Resonant Charger (RC), Commutators and Compression Heads (CH). With the exception of the compression heads, however, the changes will be virtually undetectable to users: the HVPS, RC and commutators will have the same form factors and interfaces as their predecessors, and all the modules will continue to employ a combination of air and water cooling to remove heat. Internally, the changes to these modules are incremental, but nevertheless significant. For example, the charging time for the RC has been reduced to allow higher repetition rates, and the HVPS has higher capacity. Also, the water and air cooling paths in these modules have been redesigned to improve cooling efficiencies to accommodate the higher thermal loads.

The compression heads have been increased in size to provide improved cooling as well as better resistance to corona discharge. Parasitic corona discharges can form in air in areas of high electric field, and can lead to arcing and component failures, particularly under high repetition rate continuous operation. The increased size of the XLA-300 compression heads allows a new design with significantly lowered external electric fields, thereby virtually eliminating any risk of corona discharges for robust continuous operation at very high repetition rates.

Extended operation of prototype XLA-300 SSPPM systems has demonstrated the success of these design changes. Sample data from the improved cooling design is provided in Figure 3, below. In the figure, normalized temperatures from the magnetic switching reactor cores in a 4 kHz and a prototype 6 kHz compression head are charted as a function of time. The data have all been normalized by the steady state temperature of the 4 kHz compression head core under continuous 4 kHz operation at the maximum charging voltage. The robustness of the 4 kHz compression heads has

already been amply established at Cymer[7] and in semiconductor production facilities throughout the world. The figure demonstrates that by comparison, the newly designed 6 kHz compression head runs at a significantly reduced temperature in continuous 6 kHz operation at maximum voltage in spite of the 50% higher thermal load.

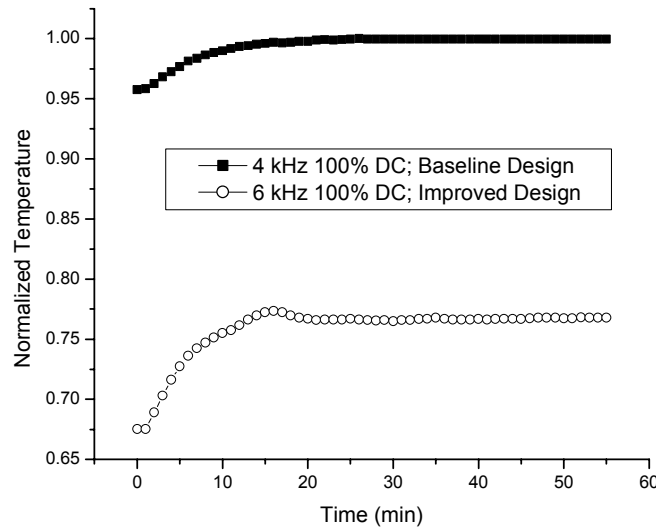


Figure 3. Comparative temperatures in the reactor cores for 4 and 6 kHz compression head designs. Note that in spite of higher repetition rate operation, the new design operates at a lower temperature.

3.2. Chamber

By far the largest fraction of the electrical energy used to produce the laser light is lost in the discharge chamber as heat. This heat is removed from the discharge chamber predominantly by a set of water-cooled internal heat exchangers, and secondarily through modest heat transfer to the air in the laser optics bay. Because the chamber temperature is controlled to a fixed setting (typically about 60 C), the heat transfer to air is constant. (During non-operation of the laser, the chamber temperature is maintained by a heater). Gas temperature regulation is maintained by varying the water flow rate through the internal heat exchangers. The maximum heat removal rate, then, is dictated by the maximum water flow rate, the water temperature, the chamber gas temperature, and the heat transfer coefficient of the heat exchanger itself.

Of course the amount of heat to be removed from the chamber depends on the laser operating conditions, and especially on the operating duty cycle and charging voltage. Figure 4a provides a contour map generated using experimental data of heat extracted from a chamber by water cooling. Note that at low duty cycle, there is little dependence on operating voltage; this is a consequence of the proportionally large fraction of heat that is generated by the fan (of the ~5.6 kW supplied to drive the fan, a substantial fraction appears as heat in the chamber, independent of laser operating conditions). As duty cycle increases, however, a larger fraction of the heat in the chamber is generated by the electrical discharge, and thus the voltage dependence becomes evident. Approximately 12 kW must be removed from the chamber at the extreme operating conditions of 75% DC, 1200V charging voltage.

Figure 4b presents an evaluation of the chamber heat exchanger efficiency, where the measured heat extraction for a range of operating conditions is compared to a heat exchanger calculation. In this case, the computed heat transfer agrees very well with measurements, where only a single adjustable parameter (namely, the friction factor for the water flow through the heat exchanger tubes) has been used to match the model to the data. From the model and data, we see that an available 10 liter/min flow rate (of 20 C water) for each chamber will be sufficient to maintain the chamber temperature at the most extreme operating conditions. This observation has already been validated through extended operation of the prototype XLA-300 system under these extreme conditions.

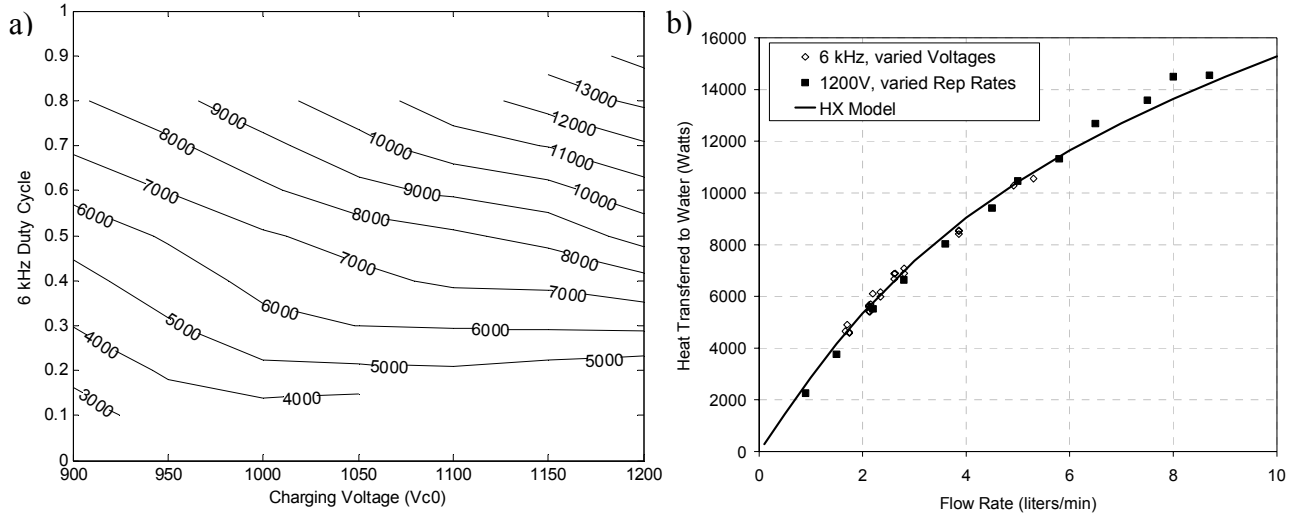


Figure 4. a) Contour map of heat extraction as a function of laser duty cycle and operating voltage. b) Comparison of modeled and measured heat transfer from a discharge chamber under various operating conditions.

4. ACOUSTIC DISTURBANCES

4.1. Acoustic wave propagation

The short-lived electric discharge used to produce laser gain also generates strong acoustic waves inside the discharge chamber that can affect the laser's performance [8,9]. The acoustic waves generated by a pulse propagate outward, reflect off of internal surfaces, and then return to the discharge volume to refract and distort the laser beam - produced by subsequent pulses. Because strong reflections are present in the discharge volume only at specific times, depending on the internal geometry of the discharge chamber, only specific repetition rates are affected. These affected repetition rates are often incorrectly termed "acoustic resonances" for convenience, in spite of the potential confusion with resonances generated by standing wave modes inside the chamber.

At low repetition rates, the interpulse interval is long enough to allow dissipation of acoustic energy so that the beam properties are generally only minimally affected. As repetition rates increase, however, acoustic reflections play a larger role in the laser beam quality. Because acoustic waves can already play a role in ultra-line narrowed laser performance above 3 kHz, the increase in repetition rate from 4 to 6 kHz brings with it substantial challenges in mitigating the deleterious effects of acoustics.

To better understand the role of acoustic waves in laser performance, the acoustic waves generated in Cymer's discharge chambers have been imaged using a shadowgraph/schlieren system aligned with the chamber's optical axis. The expanded and collimated beam of a pulsed laser is used as an illumination source in the shadowgraph/schlieren, and a gated, intensified CCD camera is used to reject the light from the discharge while imaging the discharge region. Figure 5 shows a series of shadowgraph images shortly after the discharge. The cathode is just outside the field of view at the top of the images and slightly offset to the left. The tip of the anode is visible at the bottom of the images, also offset to the left. The three images show three qualitatively distinct phases in the development of the acoustic field. First (Figure 5a), 5 usec after the discharge, clearly defined shock waves are seen propagating left and right into the undisturbed gas. Also visible in this image are vertically propagating shock waves that were generated at the electrodes themselves. Next (Figure 5b), the initial shock waves have moved out of the field of view, but multiple reflections of the vertically propagating shock waves have created a rather complex acoustic field. The dark column in the center of this image is the shadow of the gas that was ionized by the discharge itself. This volume of gas has been advected to the right away from the electrodes by the fan (recall that this volume of gas must be completely cleared from the electrodes to prevent downstream arcing and gain loss). Finally, the last shadowgraph (Figure 5c) visualizes the refractive field

that the next laser pulse would encounter, assuming a 6 kHz repetition rate. In this image, the volume of gas ionized by the previous discharge is still visible at the right, and weaker acoustic waves may still be discerned. While the dissipation of acoustic energy is evident in the series of images, acoustic waves can still be discerned at the 6 kHz delay time.

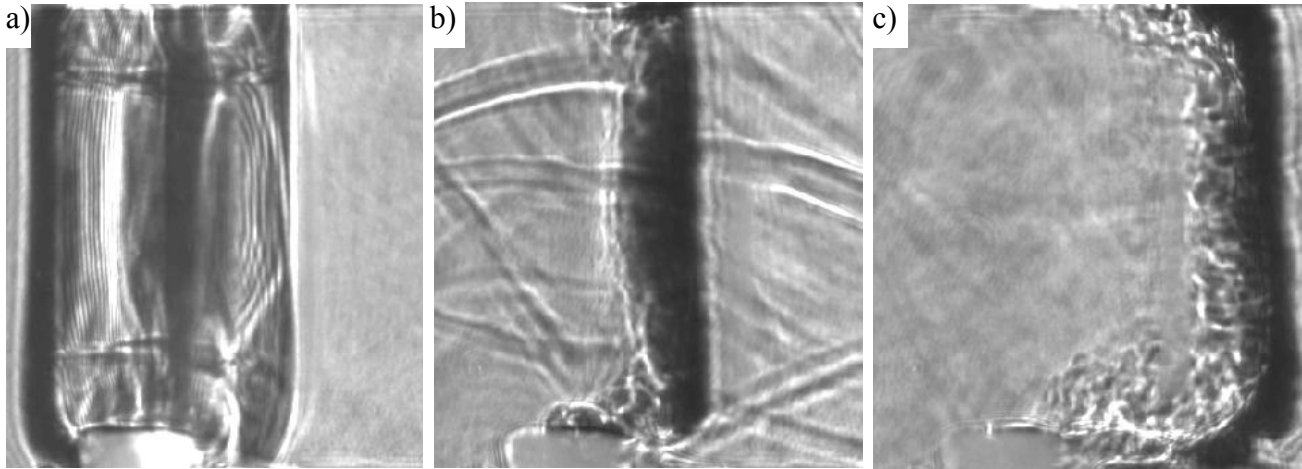


Figure 5. Shadowgraph images of the near discharge region at three delays: a) 5 usec, b) 50 usec, and c) 167 usec.

For better visualization of the weaker waves at the time delays corresponding to repetition rates of interest, a fine filament was placed vertically at the focus of a lens downstream of the discharge chamber to create a schlieren image. The schlieren image of Figure 6 was made at the same time delay as the shadowgraph of Figure 5c, and many of the same features can be identified in the two images, but with better contrast in the schlieren image. As seen in the schlieren image, the refractive field is visibly affected by multiple acoustic reflections inside the discharge chamber.

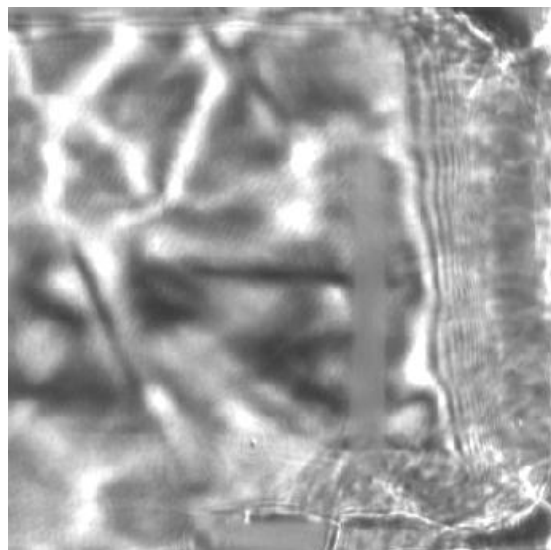


Figure 6. Schlieren image through discharge chamber at 167 usec after the discharge.

4.2. Spectral bandwidth effects

The effect that acoustic disturbances have on laser performance is demonstrated in part in Figures 7 and 8, where spectral bandwidth is charted as a function of laser repetition rate. Two metrics for bandwidth are charted from the same data: full width at half maximum (FWHM) and 95% integral of bandwidth (E95), where the effect of the measuring

spectrometer's instrument function has been removed through deconvolution for each of these measurements. It is important to note that the instrument function of the LTB ELIAS II spectrometer used for these measurements is significantly smaller than the deconvolved bandwidths (FWHM of 0.06pm, E95 of 0.2pm), which is an important prerequisite for accurate deconvolution results. We also note that these data were collected using an LNM of the XLA-100/105 design, and not with the re-designed module intended for use on the XLA-300. This results in higher baseline bandwidth performance than is expected with the new module.

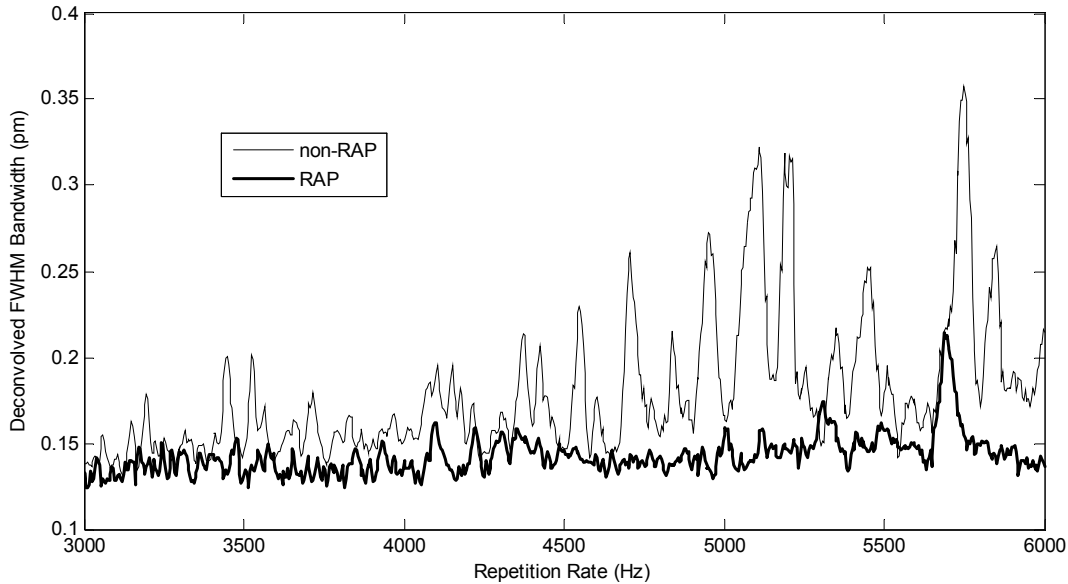


Figure 7. Deconvolved spectral bandwidth (FWHM) as a function of laser repetition rate.

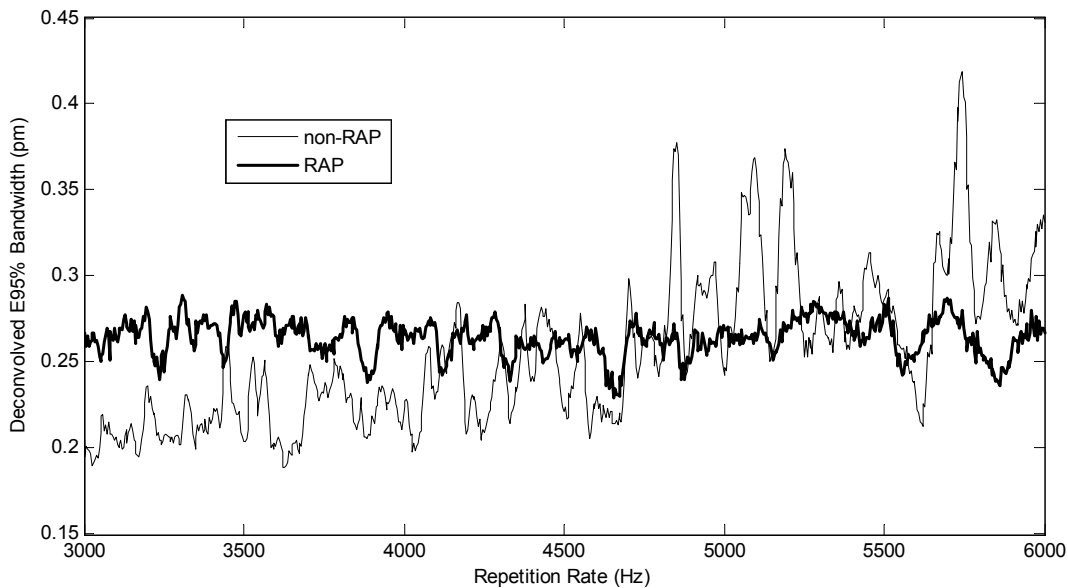


Figure 8. Deconvolved spectral bandwidth (95% integral) as a function of laser repetition rate.

Two different chamber designs are represented in Figures 7 and 8: RAP and non-RAP. As seen in the figures, many peaks in the spectral bandwidth for the non-RAP chamber cause significantly degraded performance. The acoustic origin of these peaks has been demonstrated by independent experiments. Of particular note in the non-RAP data is that

the amplitude of the acoustic peaks generally decreases with decreasing repetition rate. This is due to the dissipation of acoustic power with the increasing interpulse times discussed above.

While Cymer's RAP technology has already been applied to improve the performance of XLA-105 and XLA-200 systems at 4 kHz, the benefits RAP are particularly evident at repetition rates above 4kHz. We note that some spectral bandwidth features are still present in the RAP chamber, and mitigation/elimination of these features is a current development effort. Identification of features inside the chamber that contribute to these acoustic peaks through schlieren imagery is only one of the approaches under pursuit.

5. ENERGY STABILITY

Improved dose stability is one of the primary targets for the XLA-300 system. Clearly, then, degraded performance at the higher repetition rates cannot be accepted. One advantage for the higher repetition rates is that, for a fixed time window, more pulses can be averaged with repetition rate. Because the dominant instability in the laser pulse energies can be approximated reasonably well by a normal (gaussian) distribution, the expected dose stability improvement scales approximately as $1/\sqrt{N}$, where N represents the number of pulses in the evaluation window. To achieve an improvement, however, the width of the laser pulse energy distribution (i.e. the standard deviation) must not increase at the higher repetition rates.

Figure 9 demonstrates the intrinsic uniformity of the laser efficiency and stability across repetition rates. These data were collected using two fixed charging voltages (as indicated in the legend) that were chosen to produce nominally 10 and 15 mJ pulse energies, respectively. As seen in Figure 9a, there is very little variation in efficiency across the wide range of repetition rates investigated, and there is no loss of laser efficiency up to 6 kHz. Figure 9b presents intrinsic energy stability as measured by the usual metric of the standard deviation of pulse energy normalized by the mean pulse energy. The data collected with a 900V charging voltage (nominal 10 mJ pulse energy) show a small degradation in energy stability with increasing repetition rate above 3 kHz. But for a fixed time window, this intrinsic energy degradation is more than offset by the improvement expected from averaging a larger number of pulses at the higher repetition rates. As pulse energies are increased from 10 to 15 mJ, the pulse amplifier gain is more deeply saturated, and the deviation in pulse energies actually decreases, yielding improved stability. Furthermore, in this data, the trend toward degraded intrinsic stability at higher repetition rates appears to be suppressed at 15 mJ.

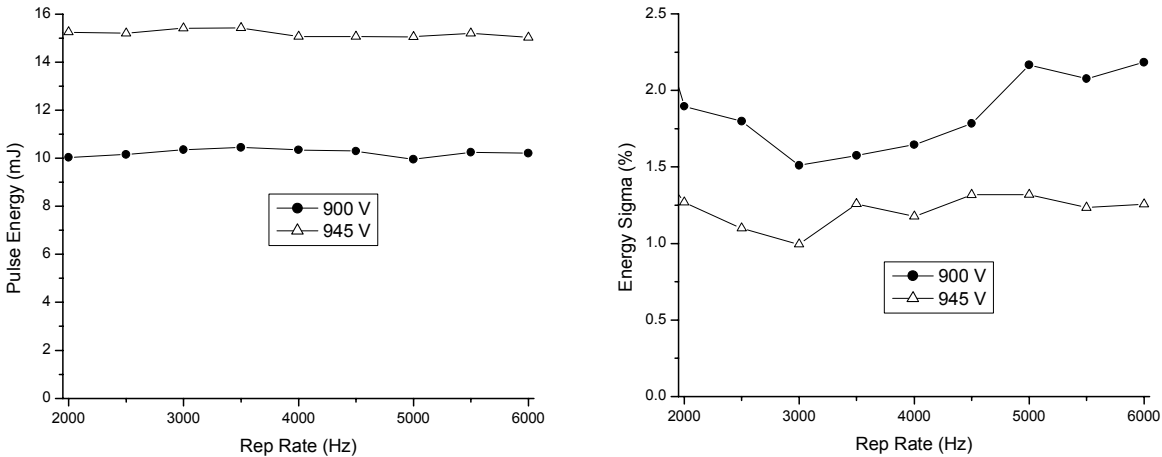


Figure 9. Pulse energy and energy stability for fixed charging voltage as a function of laser repetition rate. The charge voltages of 900 and 945 V were chosen to provide nominal pulse energies of 10 and 15 mJ, respectively, for the same nominal laser process gas mixture.

However, good intrinsic energy stability is not enough in itself to assure good dose performance: an energy feedback control system is also required. Figure 10 presents a contour chart of the maximum dose error (100% inclusion) as a function of laser pulse energy and repetition rate with the energy feedback control loop closed. The dose performance

charted was calculated using a fixed 14 ms trapezoidal time window. Except at the very lowest pulse energies and repetition rates, the target dose performance of < 0.1% is met by the prototype system.

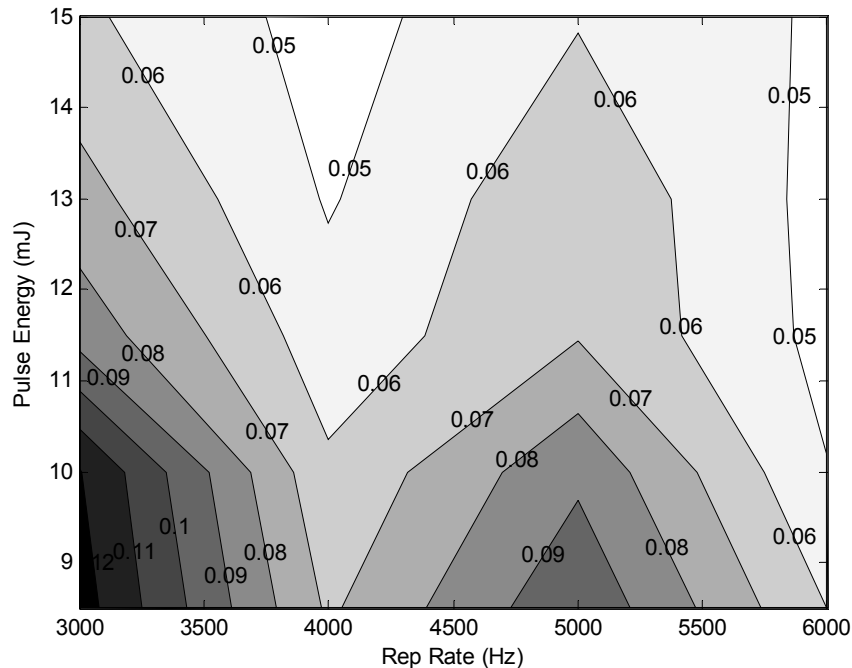


Figure 10. Maximum dose error as a function of laser repetition rate and pulse energy. 14ms trapezoidal dose window, 200ppb, 0.1 sec interburst interval

6. CONTROL SYSTEM

The controls system is divided into three main areas: Energy & Timing (E&T), wavelength, and beam judgment. The E&T control algorithm adjusts the voltage and discharge timing of the chambers in order to control the output energy of the laser. The wavelength control algorithm evaluates on-board spectral measurements and sends commands to the Line Narrowing Module (LNM) in order to adjust shot-to-shot wavelength. Beam judgment analyzes data from both the E&T control algorithm and the wavelength control algorithm in order to determine the quality of the beam on a shot-by-shot basis.

Each of these systems must operate at a higher speed for increased repetition rates. While one may expect that the processing times scale proportionally to the repetition rate, in fact, due to timing requirements for each of the hardware and software subsystems, the actual feedback processing time available for control algorithms is reduced by a factor of almost 2 when going from 4 kHz to 6 kHz. But given that microprocessor speeds have significantly outpaced laser repetition rate increases, this disproportionate reduction in processing time does not present a fundamental technology challenge, even though it can require a significant engineering effort. In the present case, the engineering effort required for the XLA platform is minimal: the XLA employs a de-centralized architecture connected by a high speed bus that provides flexibility and minimizes the rework required for system upgrades, such as high repetition rate operation.

For the XLA-300, only the wavelength/bandwidth on-board metrology hardware will require an upgrade. The wavelength control, E&T and beam judgment processing will continue to use processor boards common to the XLA-105 and XLA-200 lasers, albeit with algorithm reoptimization. The wavelength metrology subsystem is unique in this case because it employs a high resolution detector array for precise wavelength and spectral bandwidth (FWHM and E95) determination. Readout of this array at ≥ 6 kHz rates touches on the limits of Cymer's current technology, but prototype systems have already been demonstrated and will be further developed in the coming months.

7. CONCLUSIONS

The technical hurdles that limit high repetition rate operation for 193 nm ArF excimer lasers have been enumerated and addressed in this paper. The primary challenges encountered with increased repetition rate are:

- Adverse effects of discharge chamber acoustics on laser beam properties
- Laser efficiency and energy stability scaling with repetition rate
- Discharge chamber gas circulating fan power required to maintain arc-free operation
- Thermal dissipation in the pulsed power and discharge chamber modules
- Controls architecture and processing speeds for metrology and closed loop operation

The performance data presented have demonstrated that Cymer's XLA-300 laser system is well on its way to meeting these challenges and will provide superior performance for the parameters critical to the lithography process, such as spectral bandwidth and its stability, energy stability and dose control up to 6 kHz.

ACKNOWLEDGMENTS

The authors express their thanks to Tom Duffey, Herve Besaucele, Paul Melcher, Chaofeng Huang, Richard Ness, Ben Morris, Kevin Duenow and the extended XLA-300 development team for their contributions.

REFERENCES

1. V.B. Fleurö, D.J. Colon III, D.J.W. Brown, P. O'Keefe, H. Besaucele, A. Ershov, E. Trintchouk, T. Ishihara, P. Zamboni, R. Rafac, A. Lukashev, "Dual-chamber ultra line-narrowed excimer light source for 193 nm lithography," Proc. of SPIE, Vol 5040, pp. 1694-1703, 2003.
2. R. Rafac, "Overcoming limitations of etalon spectrometers used for spectral metrology of DUV excimer light sources," SPIE 29th Conference on Microlithography, Feb, 2004.
3. T. Ishihara, R. Rafac, W. Dustan, E. Trintchouk, C. Wittak, R. Perkins, R. Bergstedt, and W. Gillespie, "XLA-200: the Third-Generation ArF MOPA Light Source for Immersion Lithography," to be presented at the 29th Conference on Microlithography, Feb 27-March 4, 2005.
4. R. Sandström, A. Ershov, V. Fleurö, "MOPA Laser Architecture for High Power Lithographic Light Sources," SPIE 27th Conference on Microlithography, March 3-8, 2002.
5. V.M. Borisov, A.I. Demin, A.V. Eltsov, O.B. Khristoforov, Y.B. Kiryukhin, A.V. Prokofiev, A.Y. Vinokhodov, V.A. Vodchits, "Development of next generation excimer lasers for industrial applications," Proc. of SPIE, Vol 5137, pp.241-249, 2003.
6. T. Goto, S. Takagi, K. Kakizaki, S. Saton, S. Kosugi, T. Ohishi, Y. Kanazawa, A. Ishii, T. Teranishi, K. Yasuoka, T. Shinohe, H. Ohashi, E. Endo, K. Okamura, "Development of key components and technologies for a high repetition rate and high-power excimer laser," Review of Scientific Instruments, Vol 69 No. 1, pp. 1-9, January 1998.
7. T. Ishihara, H. Besaucele, C. Maley, V. Fleurö, P. O'Keefe, M. Haviland, R. Morton, W. Gillespie, T. Dyer, B. Moosman, R. Poole, "Long term reliable operation of a MOPA-based ArF light source for microlithography," Optical Microlithography XVII, Proc. of SPIE, Vol 5377, pp. 1858-1865.
8. K. Maeno, S. Kosugi, "On the characteristics of pressure waves in the cavity of pulsed excimer laser," SPIE Vol 3571, pp 45-51.
9. G. Imada, H. Yamao, M. Suzuki, W. Masuda, K. Yatsui, "Influence of shock waves on excitation discharge for TEA gas lasers," Proceedings of SPIE Vol 4184 (2001), pp. 423-426.